Layer-by-Layer-Processed All-Polymer Solar Cells with Enhanced Performance Enabled by Regulating the Microstructure of PYIT-OD Upper Layer

Yixuan Wu , Peng Li , Shiqi Yu , Liangang Xiao * , Yonggang Min

Posted Date: 17 May 2024

doi: 10.20944/preprints202405.1115.v1

Keywords: layer-by-layer; all-polymer solar cells; additive; morphology control; charge recombination

Article

Layer-by-Layer-Processed All-Polymer Solar Cells with Enhanced Performance Enabled by Regulating the Microstructure of PYIT-OD Upper Layer

Yixuan Wu, Peng Li, Shiqi Yu, Yonggang Min and Liangang Xiao *

School of Materials and Energy, Guangdong University of Technology, Guangzhou 510006, China
* Correspondence: xiaolg@gdut.edu.cn

Abstract: The layer-by-layer (LBL) fabrication method allows for controlled microstructure morphology and vertical component distribution, and also offers a reproducible and efficient technique for fabricating large-scale organic solar cells (OSCs). In this study, polymer D18 and PYIT-OD are employed to fabricate all-polymer solar cells (all-PSCs) using the LBL method. Morphological studies reveal that the use of additives optimizes the microstructure of the active layer, enhancing the crystallinity and charge transport capability. The optimized device with 2% CN additive significantly reduces bimolecular recombination and trap-assisted recombination. All-PSCs fabricated by the LBL method based on D18/PYIT-OD deliver a power conversion efficiency (PCE) of 15.07%. Our study demonstrates the great potential of additive engineering via LBL fabrication method in regulating microstructure of active layers, suppressing charge recombination, and enhancing the photovoltaic performance of devices.

Keywords: layer-by-layer; all-polymer solar cells; additive; morphology control; charge recombination

1. Introduction

Organic solar cells (OSCs), noted for their light weight, solution processability, and compatibility with flexible substrates, have become a focal point for researchers worldwide [1–4]. Currently, the state of the art single-junction OSCs have achieved a power conversion efficiency (PCE) exceeding 19% [5–7]. High-efficiency OSCs primarily employ the bulk heterojunction (BHJ) structure, which is spontaneously formed via phase separation from a mixed solution of electron donors and acceptor during the film deposition process. To optimize the microstructure morphology, researchers have developed a range of strategies, such as thermal annealing (TA), solvent vapor annealing (SVA), and additive engineering [8–12]. However, the photovoltaic performance of BHJ OSCs is highly dependent on molecular crystallinity, molecular orientation, phase separation, and vertical phase distribution within the active layer, which is often unpredictable and sensitive to material properties and processing conditions. This unpredictability fabrication challenges in scaling up for large-scale industrial production and limits their potential for commercial applications.

In recent years, the layer-by-layer structure, fabricated by depositing electron donor and acceptor in separate solutions, allows for controlled microstructure morphology and vertical component distribution, and also offers a reproducible and efficient technique for fabricating large-scale OSCs [13–15]. During LBL deposition process, the interfacial diffusion of electron donor and acceptor can lead to the formation of a p-i-n type structure within the active layer [16–18]. Such LBL-type devices are valued for their ease of reproducibility and reduced carrier recombination. By incorporating a wax additive to form nanoscale pores with the PM6 layer, a novel interdigitated heterojunction structure based on PM6/L8-BO bilayer heterojunction OSCs was successfully fabricated via LBL deposition method. This novel structure result to an ideal vertical phase distribution inside the active layer, leading to efficient exciton diffusion length and dissociation, and the reduced charge recombination [19]. By adjusting the solution temperature and annealing

 doi:10.20944/preprints202405.1115.v1

processes, the D18 polymer's pre-aggregation behavior in solution can be controlled, leading to manipulation of the microstructure of the D18 bottom layer. This optimized bottom layer effectively facilitates the formation of suitable networks in the L8-BO upper layer for efficient charge transport and deliver an enhanced PCE of 18.02% [20].

In the array of methods for regulating microstructure morphology of active layer, the use of additives stands out as a straightforward yet potent method to regulate the molecular packing, enhance the crystalline and improve the blend film morphology [21,22]. For the study on the additives, it is essential to delve deeper into the mechanisms how these additives influence on the film morphology evolution. For example, the introduction of a selective solvent as an additive can swell the donor domains and improve the donor-acceptor interfacial area, facilitating a more efficient charge separation and extraction processes. In addition to the chemical interactions, the physical properties of additives such as their boiling point and evaporation rate can also be critical. Solvent additive may remain in the film for a longer time during the film formation process, facilitating the molecules to self-assemble into a well-structured microstructure morphology [23,24]. The reported study have demonstrated the effectiveness of additive to fine-tune the morphology of the active layer, resulting to more ordered structure and higher charge mobility. For instance, a solvent additive of 1% 1,8-diiodoctane (DIO) was employed as the solvent additive to treat the J71:N2200 blends, resulting in more favorable phase separation and domain size. As a result, the corresponding OSCs device achieved an outstanding PCE of 9.34% with an ultrahigh fill factor (FF) of 77.86% [25]. Furthermore, by replacing DIO with diiodomethane in PM6:L8-BO based OSCs, the energetic difference between the single excited state of L8-BO and the charge transfer state in blend film was effectively reduced, while the microstructure morphology and charge transport of the optimized blend film was not deteriorated, and thereby an increased open-circuit voltage (V_{OC}) [26].

In this study, the polymers D18 and PYIT-OD were employed as donor and non-fullerene acceptor materials, respectively, for the fabrication of all-polymer solar cells (all-PSCs) using the LBL method. In addition, we systematically study how solvent additives influenced the photovoltaic performance of all-PSCs. The addition of 2% chloronaphthalene (CN) additive led to a PCE of 15.07%. This study also investigates the impact of different solvent additives on the exciton dynamics, molecular crystallinity and microstructure morphology within the D18/PYIT-OD based LBL all-PSCs devices. Our study demonstrated the great potential of additive engineering via LBL fabrication methods in regulating microstructure of active layers, suppressing carrier recombination and enhancing the photovoltaic performance of devices.

2. Result and Discussion

The chemical structure of D18 and PYIT-OD was illustrated in Figure S1. Figure 1a shows the extinction coefficient of the D18/PYIT-OD bilayer film fabricated from different processing conditions. The introduction of additives noticeably enhanced the extinction coefficient of the film, with values reaching 4.8×10^4 cm^{-1}, 6.9×10^4 cm^{-1}, and 6.1×10^4 cm^{-1} under three different processing conditions. This indicates an improvement in the molecular packing of the film due to the presence of additives. Since 585 nm is the main absorption peak of D18, our main focus is on the changes at this position under different additive conditions. The absorption peak ratio $I_{0\text{-}0}/I_{0\text{-}1}$ of the D18 film under three different processing conditions rose from 0.99 in the controlled device to 1.06 and 1.02 for bilayer films with DIO and CN additives, suggesting that the D18 film exhibited a more uniform π-π stacking with the presence of additives. The increase in crystallinity and the optimization of molecular packing are likely to enhance charge transport and photovoltaic performance. To verify whether the DIO and CN additives could enhance the photovoltaic performance of OSCs, we fabricated devices using the LBL method with a structure of ITO/PEDOT:PSS/D18/PYIT-OD/PDIN/Ag. DIO and CN additives were added to the PYIT-OD solution in measured by volume percentage. Figures 1b and S2 show the representative current density-voltage (*J*-*V*) characteristics of the devices at different concentrations of solvent additives, with specific photovoltaic parameters presented in Tables 1 and S1. The PCE for the control device (without any additive) was 12.91% with a short-circuit current density (J_{SC}) of 20.44 mA cm^{-2}, an open-circuit voltage (V_{OC}) of 0.956 V, and a

 doi:10.20944/preprints202405.1115.v1

fill factor (FF) of 66.06%. When DIO or CN additive was added, the PCE of the devices first increased and then decreased, reaching maximum PCE of 15.07% and 13.72% at 2% CN and 1% DIO concentrations, respectively. The corresponding J_{SC} was 22.00 and 21.38 mA cm^{-2}, V_{OC} was 0.969 and 0.947 V, and FF was 70.71% and 67.73%, all of which were superior to the control devices. In order to validate the accuracy of the *J-V* measurements, the external quantum efficiency (EQE) spectra for all devices were measured and illustrated in Figures 1c and S3. The J_{SC} values derived from the EQE spectra aligned with those obtained from *J-V* measurements. All devices exhibited a wide photo-response range spanning from 400 to 850 nm. In particular, when 2% CN was added into PYIT-OD solution, the EQE values between 450 to 575 nm and 725 to 825 nm were significantly higher than that of other devices.

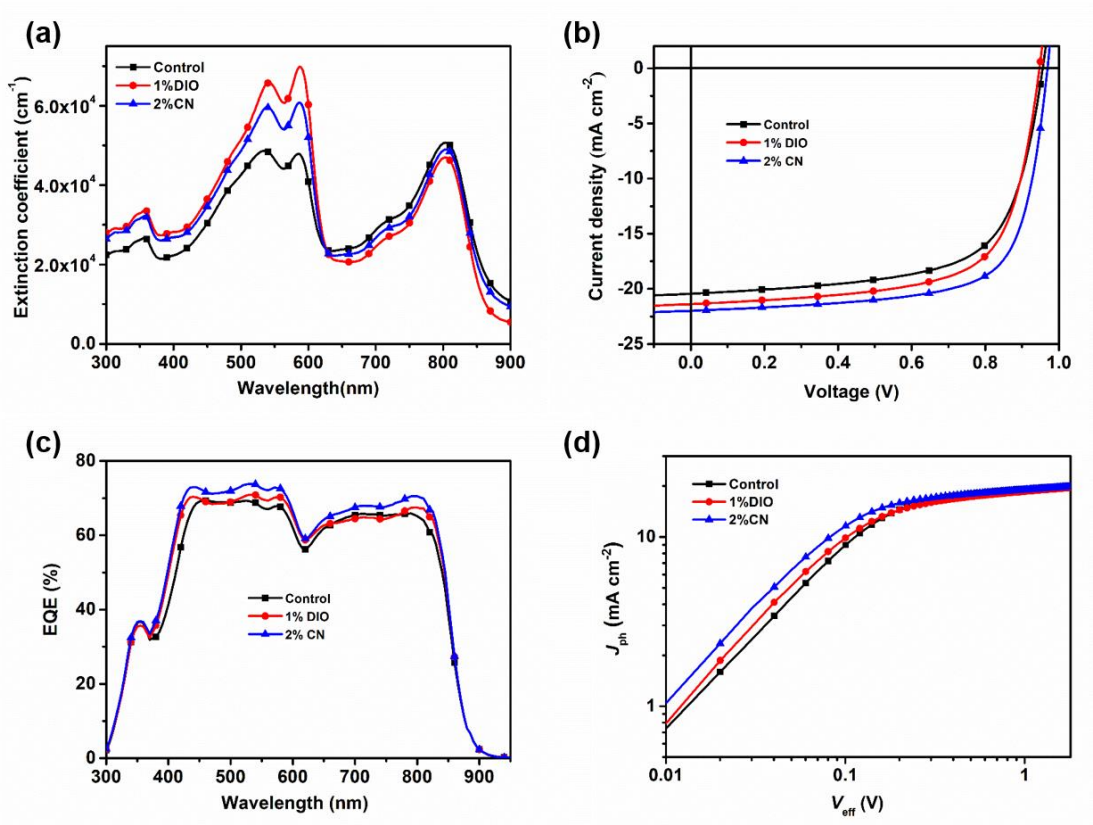

Figure 1. (a) The extinction coefficient of the D18/PYIT-OD bilayer film fabricated from different processing conditions; (b) the representative *J-V* curves of devices at different solvent additives; (c) the representative EQE spectra of devices at different solvent additives; (d) the J_{ph}-V_{eff} curves of devices at different solvent additives.

Table 1. Summary data of photovoltaic performance of devices with different solvent additives.

Condition	V_{OC} (V)	J_{SC} / J_{Cal} (mA cm^{-2})	FF (%)	PCE (%)
Control	0.956	20.44 / 19.88	66.06	12.91 (12.62)[a]
1% DIO	0.947	21.38 / 21.00	67.73	13.72 (13.43)[a]
2% CN	0.969	22.00 / 21.50	70.71	15.07(14.88)[a]

[a] Average PCE values were obtained from 10 devices.

To investigate the excitons dissociation and charge collection within devices, we conducted experiments to assess the relationship between photo-generated current (J_{ph}) and the effective voltage (V_{eff}), as shown in Figure 1d. Here, the photo-generated current (J_{ph}) and the effective voltage (V_{eff}) are calculated by J_{ph}=J_L-J_D and V_{eff}=V_0-V, respectively, where J_L and J_D refer to the current density under illumination and dark conditions, V_0 is the voltage when J_{ph} is zero, and V is the applied voltage [27,28]. Under a large V_{eff}, the J_{ph} tends to be saturated (J_{sat}), at which point nearly all excitons are

 doi:10.20944/preprints202405.1115.v1

dissociated into free carriers and collected by the electrodes [29]. We also analyzed the probability of charge dissociation (P(E,T)) of devices under different processing conditions (Table S2), which was calculated by the ratio of J_{ph} to J_{sat} under short-circuit conditions. For the devices without additives, with the addition of 1% DIO additive and 2% CN additive, the P(E,T) values were 89.3%, 91.4%, and 94.9%, respectively. Based on the equation $J_{sat}=qG_{max}L$, we calculated the corresponding maximum exciton generation rates (G_{max}) was to be 1.31×10^{28}, 1.32×10^{28}, and 1.38×10^{28} m^{-3} s^{-1}, respectively. Devices with 2% CN additive showed increased G_{max}, which correlated well with their higher J_{SC}, potentially contributing to the improved light absorption and more orderly molecular packing. These results demonstrate that devices with 2% CN additive exhibit superior performance in exciton and charge dynamics.

To delve into the charge recombination in different devices, we performed *J-V* under various light intensities (P_{light}) and plotted the correlation curves of J_{SC} and V_{OC} with P_{light}. The relationship between J_{SC} and P_{light} follows the formula $J_{SC}\propto(P_{light})^S$, where S reflects the intensity of bimolecular recombination in the device. Generally, The S value being very close to the unit suggests that OSC devices experience minimal bimolecular recombination [30]. As shown in Figure 2a, for devices without additive, with 1% DIO additive, and with 2% CN additive, the corresponding S values are 0.96, 0.97, and 0.98, respectively. The results indicate that devices based on D18/PYIT-OD with 2% CN are most effective in suppressing bimolecular recombination. Meanwhile, the V_{OC} versus P_{light} curves were shown in Figure 2b, the controlled device exhibited the highest fitting slope, suggesting severe trap-assisted Shockley-Read-Hall (SRH) or bimolecular recombination. For the device with 1% DIO additives and 2% CN additives, the slopes were decreased to 1.60 kBT/q and 1.52 kBT/q, respectively. The smallest fitting slope for the device with CN additive indicated that SRH or bimolecular recombination is effectively suppressed, promoting effective charge transport and collection.

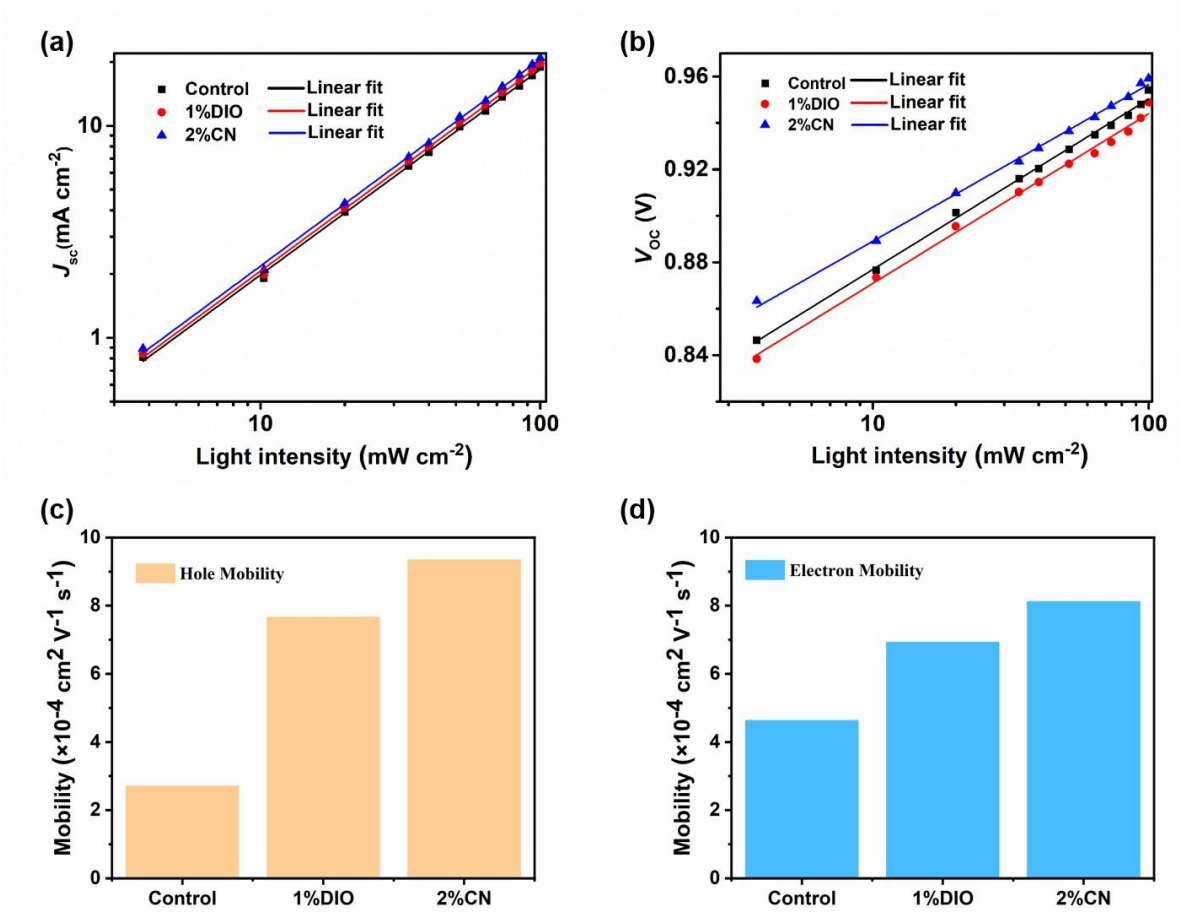

Figure 2.

 doi:10.20944/preprints202405.1115.v1

Single carrier devices based D18/PYIT-OD bilayer films were fabricated to investigate the charge transport behavior by the space charge-limited current (SCLC) method [31], and summarized data was listed in Table S3. The specific device structure for the hole-only device is ITO/PEDOT:PSS/D18/PYIT-OD/Ag, while the electron-only device is ITO/ZnO/D18/PYIT-OD/PFN-Br/Ag. As shown in Figure 2c,d, the hole mobility (μ_h) and electron mobility (μ_e) for the device without additive are 3.71×10^{-4} cm^2 V^{-1} s^{-1} and 4.63×10^{-4} cm^2 V^{-1} s^{-1}, respectively. After adding additives to PYIT-OD, the measured μ_h increased to 7.66×10^{-4} cm^2 V^{-1} s^{-1} (1% DIO) and 9.34×10^{-4} cm^2 V^{-1} s^{-1} (2% CN), while the μ_e increased to 6.93×10^{-4} cm^2 V^{-1} s^{-1} (1% DIO) and 8.18×10^{-4} cm^2 V^{-1} s^{-1} (2% CN). It is evident that the device treated with 2% CN additive not only has more efficient charge transport performance but is also more balanced charge transport, indicating an effective reduction in charge accumulation and recombination, thereby improving the J_{SC} of devices. In addition, exciton separation and charge transfer at the electron donor and acceptor interface are crucial for device photovoltaic performance. To investigate the exciton separation and charge transfer of bilayer films, we performed steady-state photoluminescence (PL) spectra of the pristine D18 film and the D18/PYIT-OD bilayer films, as shown in Figure S4. The films were excited at 467 nm, and D18 exhibited typical emission peaks at 620 and 680 nm. The PL intensity at these emission peaks was significantly quenched in the D18/PYIT-OD bilayer films, indicating efficient charge transfer at the electron donor and acceptor interface. For the bilayer film with added 2% CN, this PL quenching is most pronounced, indicating most efficient charge transfer.

We used atomic force microscopy (AFM) to observe the influence of additives type and their concentrations on the surface morphology of bilayer films. As shown in Figure 3, the root-mean-square (RMS) roughness value is 1.68 nm for the bilayer film without any additive. With increasing DIO concentration from 0.5% to 2%, RMS roughness values rose from 1.87 nm to 3.43 nm. When the CN concentration increased from 1% to 2%, the RMS roughness values slightly decreased from 1.70 nm to 1.54 nm, exhibiting a more refined structure. However, excessive additive (3% CN concentration) led to large-scale aggregation, resulting in a sharp increase in film RMS roughness, which severely damaged device efficiency. Additionally, by examination of the transmission electron microscopy (TEM) images for both the controlled film and those added with 1% DIO and 2% CN (Figure 4), it becomes apparent that these additives precipitate morphological inhomogeneity within the film, likely attributable to the induced crystallization. Comparative analysis indicates that the addition of 2% CN results in a more uniform and fiber-like film structure, leading to higher FF in the corresponding devices. This also aids in effective separation of excitons and charge transport.

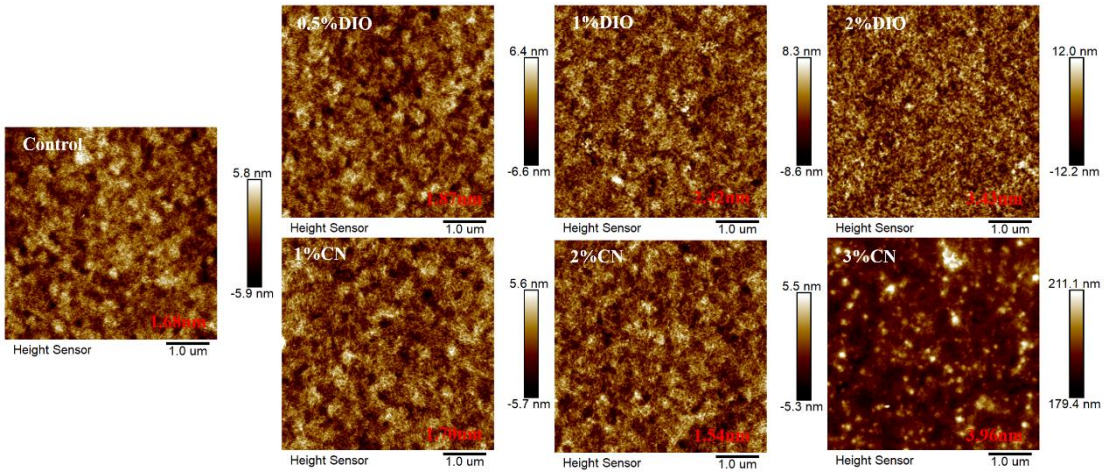

Figure 3. AFM images of bilayer films based on D18/PYIT-OD under different processing conditions.

 doi:10.20944/preprints202405.1115.v1

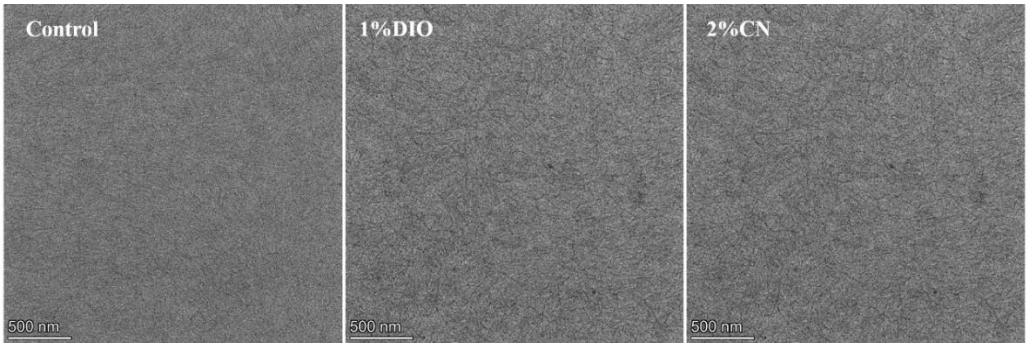

Figure 4. TEM images of bilayer films based on D18/PYIT-OD under different processing conditions.

To gain a deeper understanding of the molecular packing and crystalline properties within the active layer, we utilized grazing-incidence wide-angle X-ray scattering (GIWAXS) measurements to examine the D18/PYIT-OD bilayer films under various processing conditions. Figure 5a shows the 2D GIWAXS patterns of D18/PYIT-OD bilayer films without any additive (control), with 1% DIO, and with 2% CN. The corresponding line-cut plots in the in-plane (IP) and out-of-plane (OOP) directions were shown in Figure 5b,c, respectively. From the GIWAXS 2D GIWAXS patterns under three different processing conditions, we observed a strong (010) π-π stacking peak in the OOP direction and a distinct (100) lamellar stacking peak in the IP direction, This indicates that D18/PYIT-OD bilayer films predominantly exhibited a face-on orientation. This result also implied that fabrication the upper layer of PYIT-OD does not significantly alter the molecular orientation of the D18 film [32]. For the bilayer film with 1% DIO, the diffraction peak intensities are more pronounced for both the IP lamellar stacking and the OOP π-π stacking. In addition, It is evident that the bilayer film containing 2% CN exhibits a minimum full width at half maximum (FWHM) value of 0.292 Å at 1.69 $Å^{-1}$ in the OOP direction, indicating a strong π-π stacking. In comparison, the FWHM values for the controlled bilayer film and the film with 1% DIO are 0.352 Å and 0.317 Å, respectively. The reduced FWHM value in the film with 2% CN suggests a higher crystal coherence length (CCL). A larger CCL suggested an increase in the number of crystal repeating units within the active layer, which is more conducive to the charge transport. This is consistent with the results above where the OSC device containing 2% CN exhibited the highest hole and electron mobility. The bilayer film that incorporated the 1% DIO additive suffered from excessive aggregation, leading to compromised photovoltaic performance of the OSC device.

 doi:10.20944/preprints202405.1115.v1

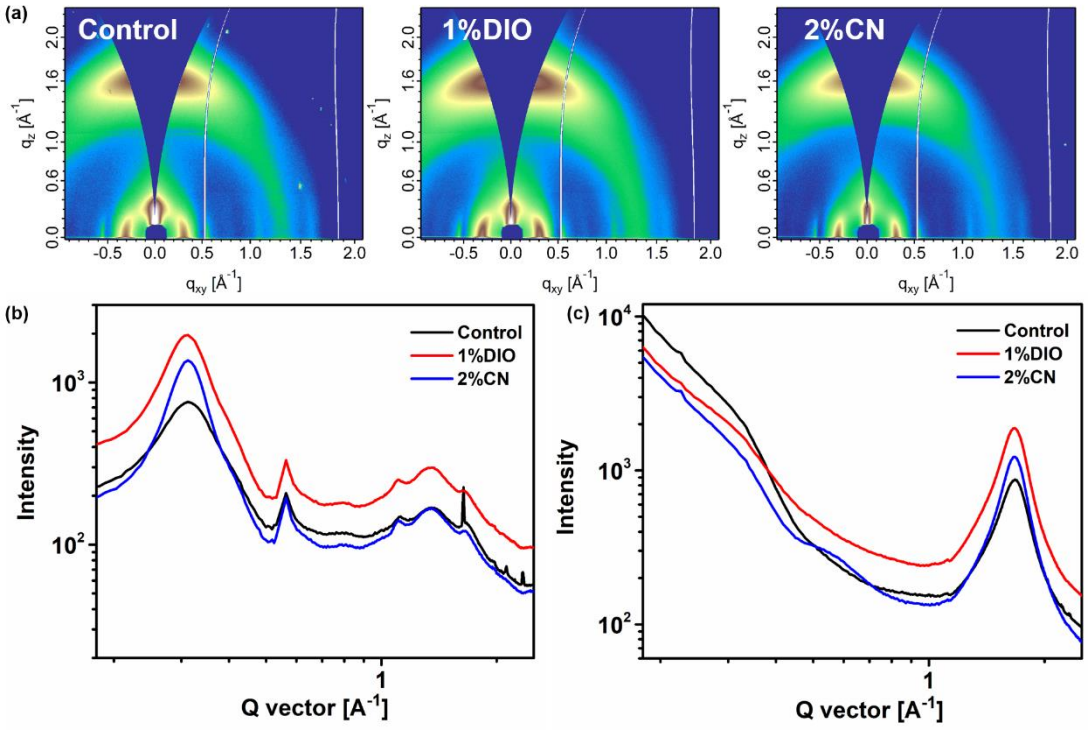

Figure 5. (a) 2D GIWAXS patterns of bilayer films based on D18/PYIT-OD under different processing conditions; GIWAXS line-cuts of bilayer films based on D18/PYIT-OD under different processing conditions (b) in the in-plane direction and (c) in the out-of-plane direction.

3. Conclusion

In conclusion, LBL all-PSCs based on the D18/PYIT-OD were fabricated by incorporating solvent additives into the PYIT-OD acceptors to regulate the appropriate microstructure. CN and DIO additives have a significant impact on the molecular packing and morphology of the active layer. With the optimized amount of additives, both CN and DIO can significantly enhance the photovoltaic performance of the devices, particularly CN, which is very effective in improving the J_{SC} and FF. The existence of additives also affect the crystallization and packing of D18, thereby affecting the charge mobility of the devices. In addition, devices containing 2% CN additive result in a significant increase in exciton separation, and a marked reduction in bimolecular recombination and trap-assisted recombination. Finally, a morphological study confirms that the existence of additives significantly improves the molecular crystallization and packing of the active layer, resulting in enhanced crystallinity and CCL. As a result, the optimized LBL all-PSCs based on the D18/PYIT-OD delivered a high PCE of 15.07%. The strategy of separately regulating the morphology of the electron donor and acceptor layers via the LBL fabrication method makes it a very promising approach to promote the development of organic photovoltaic technology.

Conflicts of interest: There are no conflicts to declare.

Acknowledgments: L. X. and was supported by the financial support from the National Natural Science Foundation of China (51903057) and the Guangzhou Basic and Applied Basic Research Foundation (2023A04J0349). We also thank the support from the National Key Research and Development Program of China (2020YFB0408100) and Analysis and Test Center of Guangdong University of technology for the UV-vis-NIR and PL spectroscopy measurement.

References

1. Xiao, L.; Wu, X.; Ren, G.; Kolaczkowski, M. A.; Huang, G.; Tan, W.; Ma, L.; Liu, Y.; Peng, X.; Min, Y., *Adv. Funct. Mater.* **2021,** *31* (41), 2105304.
2. Yi, J.; Zhang, G.; Yu, H.; Yan, H., *Nat. Rev. Mater.* **2024,** *9* (1), 46-62.

3. Peng, S.; Luo, J.; Li, P.; Xiao, L.; Yang, C.; Jin, Y.; Lin, R.; Huo, Y.; Liu, Y.; Min, Y., *Chem. Eng. J.* **2023,** *474*, 145501.
4. Zhang, H.; Jia, S.; Liu, Z.; Chen, Z., *Molecules* **2023,** *28* (19), 6832.
5. Han, C.; Wang, J.; Zhang, S.; Chen, L.; Bi, F.; Wang, J.; Yang, C.; Wang, P.; Li, Y.; Bao, X., *Adv. Mater.* **2023,** *35* (10), 2208986.
6. Zhu, L.; Zhang, M.; Xu, J.; Li, C.; Yan, J.; Zhou, G.; Zhong, W.; Hao, T.; Song, J.; Xue, X., *Nat. Mater.* **2022,** *21* (6), 656-663.
7. Liu, K.; Jiang, Y.; Liu, F.; Ran, G.; Huang, F.; Wang, W.; Zhang, W.; Zhang, C.; Hou, J.; Zhu, X., *Adv. Mater.* **2023,** *35* (32), 2300363.
8. Xiao, L.; Li, Z.; Hu, Q.; Liu, Y.; Zhong, W.; Mei, X.; Russell, T. P.; Liu, Y.; Min, Y.; Peng, X., *J. Mater. Chem. C.* **2019,** *7* (31), 9618-9624.
9. Xiao, L.; Yan, C.; Li, Z.; Zhong, W.; Tan, W.; Liu, Y.; Liu, F.; Peng, X.; Min, Y., *Acs. Appl. Energ. Mater.* **2021,** *4* (4), 4234-4241.
10. McDowell, C.; Abdelsamie, M.; Toney, M. F.; Bazan, G. C., *Adv. Mater.* **2018,** *30* (33), 1707114.
11. Meng, L.; Wu, S.; Wan, X.; Shen, Z.; Li, M.; Yang, Y.; Wang, J.; Lu, G.; Ma, Z.; Yao, Z., *Chem. Mater.* **2022,** *34* (7), 3168-3177.
12. Hou, Y.; Wang, Q.; Huang, C.; Yang, T.; Shi, S.; Yao, S.; Ren, D.; Liu, T.; Zhang, G.; Zou, B., *Molecules* **2022,** *27* (17), 5713.
13. Li, X.; Du, X.; Zhao, J.; Lin, H.; Zheng, C.; Tao, S., *Sol. RRL* **2021,** *5* (1), 2000592. DOI https://doi.org/10.1002/solr.202000592.
14. Li, M.; Wang, Q.; Liu, J.; Geng, Y.; Ye, L., *Mater. Chem. Front.* **2021,** *5* (13), 4851-4873. DOI 10.1039/D1QM00407G.
15. Wei, Y.; Chen, Z.; Lu, G.; Yu, N.; Li, C.; Gao, J.; Gu, X.; Hao, X.; Lu, G.; Tang, Z., *Adv. Mater.* **2022,** *34* (33), 2204718.
16. Chen, H.; Zhao, T.; Li, L.; Tan, P.; Lai, H.; Zhu, Y.; Lai, X.; Han, L.; Zheng, N.; Guo, L.; He, F., *Adv. Mater.* **2021,** *33* (37), 2102778. DOI https://doi.org/10.1002/adma.202102778.
17. Li, X.; Yang, H.; Du, X.; Lin, H.; Yang, G.; Zheng, C.; Tao, S., *Chem. Eng. J.* **2023,** *452*, 139496.
18. Zhang, Y.; Wu, B.; He, Y.; Deng, W.; Li, J.; Li, J.; Qiao, N.; Xing, Y.; Yuan, X.; Li, N., *Nano Energy* **2022,** *93*, 106858.
19. Xu, X.; Yu, L.; Meng, H.; Dai, L.; Yan, H.; Li, R.; Peng, Q., *Adv. Funct. Mater.* **2022,** *32* (4), 2108797. DOI https://doi.org/10.1002/adfm.202108797.
20. Wu, X.; Wu, Y.; Peng, S.; Xiao, L.; Xiao, Z.; Zhang, W.; Ren, G.; Min, Y.; Liu, Y., *Sol. RRL* **2023,** *7* (11), 2300136.
21. Yang, X.; Li, B.; Zhang, X.; Li, S.; Zhang, Q.; Yuan, L.; Ko, D. H.; Ma, W.; Yuan, J., *Adv. Mater.* **2023,** *35* (24), 2301604.
22. Ma, Y.-F.; Zhang, Y.; Zhang, H.-L., *J. Mater. Chem. C.* **2022,** *10* (7), 2364-2374.
23. Song, X.; Gasparini, N.; Baran, D., *Advanced Electronic Materials* **2018,** *4* (10), 1700358.
24. Li, Z.; Yan, C.; Xiao, L.; Mao, H.; Liu, J.; Tan, W.; Min, Y., *Org. Electron.* **2021,** *93*, 106135.
25. Liu, X.; Li, X.; Wang, L.; Fang, J.; Yang, C., *Nanoscale* **2020,** *12* (8), 4945-4952. DOI 10.1039/C9NR10495J.
26. Song, J.; Zhu, L.; Li, C.; Xu, J.; Wu, H.; Zhang, X.; Zhang, Y.; Tang, Z.; Liu, F.; Sun, Y., *Matter* **2021,** *4* (7), 2542-2552.
27. Ma, Y.; Cai, D.; Wan, S.; Wang, P.; Wang, J.; Zheng, Q., *Angew. Chem. Int. Edit.* **2020,** *132* (48), 21811-21817.
28. Hu, K.; Du, J.; Zhu, C.; Lai, W.; Li, J.; Xin, J.; Ma, W.; Zhang, Z.; Zhang, J.; Meng, L.; Li, Y., *Sci. Chi. Chem.* **2022,** *65* (5), 954-963. DOI 10.1007/s11426-022-1219-7.
29. Xiao, L.; He, B.; Hu, Q.; Maserati, L.; Zhao, Y.; Yang, B.; Kolaczkowski, M. A.; Anderson, C. L.; Borys, N. J.; Klivansky, L. M., *Joule* **2018,** *2* (10), 2154-2166.
30. Dong, S.; Zhang, K.; Liu, X.; Yin, Q.; Yip, H.-L.; Huang, F.; Cao, Y., *Sci. Chi. Chem.* **2019,** *62*, 67-73.
31. Xiao, L.; Kolaczkowski, M. A.; Min, Y.; Liu, Y., *ACS. Appl. Mater. Interfaces* **2020,** *12* (37), 41852-41860.
32. Xiao, M.; Meng, Y.; Tang, L.; Li, P.; Tang, L.; Zhang, W.; Hu, B.; Yi, F.; Jia, T.; Cao, J.; Xu, C.; Lu, G.; Hao, X.; Ma, W.; Fan, Q., *Adv. Funct. Mater.* **2024,** *34* (13), 2311216. DOI https://doi.org/10.1002/adfm.202311216.